Industrial Chemistry & Materials

工业化学与材料 (英文)
(Online) ISSN 2755-2500
(Print) ISSN 2755-2608
CN 10-2056/TQ
rsc.li/icm

Volume 4 Number 1 January 2026

PAPER
Ryan P. Lively, Christopher W. Jones *et al.*
Amine-dependent CO_2 sorption on amine-impregnated Mg_2(dobpdc) MOF under humid conditions

ROYAL SOCIETY OF CHEMISTRY

ICM Industrial Chemistry & Materials

Industrial Chemistry & Materials

ROYAL SOCIETY OF CHEMISTRY

PAPER

View Article Online
View Journal | View Issue

Check for updates

Cite this: *Ind. Chem. Mater.*, 2026, **4**, 52

Amine-dependent CO_2 sorption on amine-impregnated Mg_2(dobpdc) MOF under humid conditions†

MinGyu Song,[a] Guanhe Rim,[a] Ghazal Mirzazadeh,[b] Jacob Hoffman,[a] Hyun June Moon,[a] Johannes E. Leisen,[c] Omid Ghaffari Nik,[d] Ryan P. Lively *[a] and Christopher W. Jones *[ac]

Amine-functionalized Mg_2(dobpdc) sorbents are prepared and studied systematically using three amines of different sizes: *N*,*N*′-dimethylethylenediamine (m-2-m), tetraethylenepentamine (TEPA), and poly(ethyleneimine) (PEI), in order of increasing size. A prototypical amine-appended Mg-based metal–organic framework, m-2-m-Mg_2(dobpdc), is tested under dry direct air capture (DAC) conditions at cold temperatures (<25 °C) with the objective of increasing the CO_2 capture fraction by shifting the step pressure in the isotherm to lower pressures. We observe that the theoretical amine efficiency (one CO_2 to one diamine) could not be achieved due to the failure of the established amine insertion mechanism. In contrast, TEPA-impregnated Mg_2(dobpdc) shows a significant increase in its CO_2 adsorption capacity under humid conditions (3.9 mmol g^{-1} and 0.33 amine efficiency at 25 °C) compared to dry conditions (0.54 mmol g^{-1}), aided by hydration of amines by water at elevated relative humidities (≥50% RH), which frees some amine chains and alleviates diffusion resistances along the MOF pore. On the other hand, both branched and linear PEI-impregnated Mg_2(dobpdc) samples undergo morphological degradation after humid adsorption/desorption cycles, likely due to the ineffective protection of the open metal sites in the MOF from water by the higher molecular weight amines. While degradation of PEI-impregnated Mg_2(dobpdc) raises a concern about the overall stability of poly(amine)-impregnated Mg_2(dobpdc) materials, the TEPA-impregnated sample shows stable performance over 20 humid sorption/desorption cycles with N_2 purge for desorption and over 8 humid cycles with vacuum desorption.

Received 7th January 2025,
Accepted 27th April 2025

DOI: 10.1039/d5im00002e

rsc.li/icm

Keywords: Direct air capture; Humidity; Metal organic frameworks; DAC; Hydration; Degradation.

1 Introduction

In the past decades, solid amine materials have been at the center of focus by researchers aiming to develop energy efficient CO_2 capture materials.[1] Among different amines, polymeric or oligomeric amines such as poly(ethyleneimine) (PEI) and tetraethylenepentamine (TEPA) have been intensively studied using various porous inorganic supports. For example, the concept of the molecular basket, *i.e.*, amine impregnation in the pores of ordered porous materials, was first introduced by Xu *et al.* using mesoporous silica MCM-41, followed by expansion of the concept to amine impregnated mesoporous carbons and metal–organic frameworks (MOF) such as MIL-101(Cr), amongst other supports.[2–4] These amine impregnated sorbents typically show IUPAC type 1 isotherms, suggesting strong interaction between the amines and CO_2 even at ultra dilute CO_2 concentrations. While their adsorption mechanism is based on the direct interaction between amines and CO_2, a novel CO_2 adsorption mechanism was discovered in amine-appended Mg_2(dobpdc), where a CO_2 molecule is inserted between the metal in the framework and a pendant diamine bound to the open metal site of the framework.[5] The CO_2 insertion mechanism endowed amine-appended Mg_2(dobpdc) with a unique step adsorption isotherm with record high amine efficiency (one CO_2 to one diamine). Later, Siegelman *et al.* reported that the step pressure of amine-appended Mg_2(dobdpc) can be controlled by the choice of amines, which influences the strength of the interaction between the amine

[a] *School of Chemical & Biomolecular Engineering, Georgia Institute of Technology, Atlanta, GA 30332, USA. E-mail: ryan.lively@chbe.gatech.edu, cjones@chbe.gatech.edu*
[b] *School of Computer Science, Georgia Institute of Technology, Atlanta, GA 30332, USA*
[c] *Department of Chemistry and Biochemistry, Georgia Institute of Technology, Atlanta, GA 30332, USA*
[d] *CarbonCapture Inc., 1242 Palmetto St, Los Angeles, California 90013, USA*
† Electronic supplementary information (ESI) available. See DOI: https://doi.org/10.1039/d5im00002e

and Mg open metal site.[6] The resulting *N*,*N*′-dimethylethylenediamine (m-2-m) functionalized Mg_2(dobpdc) and *N*,*N*-diisopropylethylenediamine (ii-2) functionalized Mg_2(dobpdc) have step pressures at <10 mbar and ~300 mbar in their 25 °C isotherms, respectively. In parallel, tetraamine-appended Mg_2(dobpdc) showed outstanding stability under flue gas adsorption and steam regeneration conditions over 1000 cycles after optimizing the length of the amine to have two amine-open metal site bindings across the pore diameter of Mg_2(dobpdc).[7]

Even though different combinations of amines with Mg_2(dobpdc) demonstrated excellent CO_2 adsorption capacity and potential for energy efficient regeneration under flue gas CO_2 capture conditions (≥10 mbar CO_2) by swinging across a narrow window of temperature or pressure between the adsorption onset temperature or pressure,[6] studies related to the DAC partial pressure region (~0.4 mbar CO_2) remain rare. This is likely because of the disadvantages of amine-appended Mg_2(dobpdc) materials for DAC conditions, such as their low CO_2 capture fraction (captured CO_2/flowed CO_2) in a dynamic adsorption system, as reported by Darunte *et al.*[8] As commercial scale DAC requires fast flow velocities, typically in excess of ~1 m s^{-1}, the flow rate dependence of the carbon capture fraction limits the practicality of these particular amine-appended MOFs in DAC. Bose *et al.* did demonstrate 400 ppm CO_2 adsorption cycles using m-2-m-Mg_2(dobpdc), but the thermogravimetric method deployed in the research did not provide a meaningful carbon capture fraction under DAC conditions due to its non-ideal gas flow path.[9]

In this study, we show how different amine sizes and structures influence the 400 ppm CO_2 adsorption capacity and sorbent stability under various DAC conditions, providing mechanistic insights into enhanced or compromised CO_2 adsorption behavior. We prepared amine-functionalized Mg_2(dobpdc) materials with amines of three different sizes, m-2-m, TEPA, and PEI. A hypothesis was made that deploying amine-appended Mg_2(dobpdc), specifically m-2-m-Mg_2(dobpdc), in cold regions for DAC could enhance its carbon capture fraction due to the increased thermodynamic driving force for adsorption and potentially, increased rates thanks to its reportedly inverse Arrhenius kinetics (faster kinetics at lower temperatures) as communicated by Martell *et al.*[10] We studied the 400 ppm CO_2 capture behavior of amine appended Mg_2(dobpdc) under a wide range of temperatures from −20 to 25 °C. As expected, lower temperatures shifted the adsorption onset pressure of the amine appended Mg_2(dobpdc) adsorbents to lower values due to the exothermic nature of gas adsorption. However, breakthrough profiles for m-2-m-Mg_2(dobpdc) from −20 to 25 °C showed similar adsorption capacities. In the literature, the slow adsorption kinetics of amine appended Mg_2(dobpdc) has been previously reported.[8,10,11] Martell *et al.* observed a minimal CO_2 uptake for a certain time period at the beginning of 100 or 15 mol% CO_2 adsorption in a gravimetric adsorption system.[10] With thorough adsorption and spectroscopic studies, they suggested that this long induction period of amine-appended Mg_2(dobpdc) was due to the slow formation of metal-bound ammonium carbamate chains (CO_2 insertion mechanism) after relatively faster non-metal-bound ammonium carbamate formation as a first step.[10] Therefore, we attributed the insignificant adsorption capacity difference at different adsorption temperatures to the intrinsically slow kinetics or failure of initiating the CO_2 insertion mechanism of amine-appended Mg_2(dobpdc) under our ultra dilute (400 ppm and dry) CO_2 concentration.[8,10,11] For the sake of conciseness, detailed results and discussion about amine-appended Mg_2(dobpdc) for DAC are available in the ESI.†

To address the obstacles originating from the CO_2–amine insertion mechanism, oligomeric (TEPA) and polymeric amine (PEI) impregnated Mg_2(dobpdc) materials were also synthesized, seeking to rectify the low CO_2 capture fraction of amine-appended Mg_2(dobpdc) under DAC conditions. A high CO_2 capture fraction reported by Cao *et al.* using TEPA-appended Mg_2(dobdc) under 15 vol% CO_2 (fixed bed breakthrough) suggests a similarly high capture fraction might be realized in TEPA-impregnated Mg_2(dobpdc) systems for DAC.[12] While focusing on flue gas CO_2 capture, isotherms presented by Choe *et al.* display increased CO_2 uptake at low partial pressure (isotherms) with higher TEPA loading in TEPA-appended Mg_2(dobpdc) adsorbent, validating a high loading of amines in Mg_2(dobpdc) as a suitable strategy for DAC application.[13] Here, we observe that TEPA-impregnated in Mg_2(dobpdc) enabled a high carbon capture fraction and elimination of the flow rate dependency of 400 ppm CO_2 capture of the amine-appended materials. Although the TEPA-impregnated Mg_2(dobpdc) showed diffusion-limited CO_2 adsorption behavior in its breakthrough curves under dry conditions, using a humidity above the stoichiometric amine hydration level (water/amine = 1.0 at ≥50% RH) alleviated much of the resistance to CO_2 diffusion. Moreover, *in situ* IR and desorption studies revealed that the hydration of the amines allows deeper penetration of CO_2 through the amine film, resulting in a delayed CO_2 desorption peak with increased humidity under temperature programmed desorption (TPD) conditions. Unexpectedly, branched or linear poly(ethyleneimine) (BPEI or LPEI, respectively) (~800 g mol^{-1}) impregnated Mg_2(dobpdc) materials showed substantial degradation in their CO_2 adsorption capacities and particle morphology after humid cycles, likely due to the ineffective protection of the Mg_2(dobpdc) open metal sites using these large polyamines. In contrast, further investigation of TEPA-impregnated Mg_2(dobpdc) demonstrated its stability under repeated humid DAC cycles under N_2 purge and more realistic vacuum desorption conditions. The structure of the amine plays a defining role in the utility, or lack thereof, of the Mg_2(dobpdc) based adsorbents.

2 Results and discussion

In our initial study of amine-appended Mg_2(dobpdc) under dry DAC conditions at low temperatures, we observed that

the CO_2 insertion mechanism did not proceed (data and discussion available in the ESI,† Section 2). To overcome the observed low adsorption capacity, low carbon capture fraction, and flow rate dependence of the amine appended Mg_2(dobpdc) for DAC,[8] two different sizes of amines, tetraethylenepentamine (TEPA) and poly(ethyleneimine) (PEI), were used to functionalize Mg_2(dobpdc) by a traditional impregnation method. Although both TEPA and PEI impregnated Mg_2(dobpdc) showed improved CO_2 uptake under humid conditions compared to dry conditions (data available in ESI†), their adsorption behavior and stability under humid adsorption/desorption experiments were dissimilar. The presence of bulky amines in a narrow pore can cause significant CO_2 diffusion resistance and reduced amine availability.[14] Furthermore, some larger amines may not efficiently protect open metal sites in the Mg_2(dobpdc) framework due to steric constraints and lead to the hydrolysis of the framework under humid conditions, as shown in Fig. 1. To this end, in the following section, we focus on the causes of their differing adsorption and degradation behaviors under humid conditions.

Increased CO_2 adsorption capacity of oligomeric amine impregnated-Mg_2(dobpdc) under humid DAC conditions: hydration of amines enables amine availability

The CO_2 adsorption capacities of TEPA-impregnated Mg_2(dobpdc) materials had a strong dependence on the relative humidity (RH) at 25 °C. In this section, this behavior was investigated by fixed bed breakthrough experiments under dry and humid conditions, measurement of single component H_2O isotherms, both *via in situ* IR spectroscopy and *via* temperature programmed desorption (TPD) studies.

Cyclic TSA breakthrough experiments under various humidities at 25 °C were conducted to investigate the CO_2 adsorption behavior and the stability of the materials under different humidities. The CO_2 adsorption capacity fractions, defined as CO_2 adsorption in each cycle divided by the initial CO_2 adsorption capacity, and the corresponding breakthrough profiles for each cycle, are shown in Fig. 2 and S16.† We note that the CO_2 adsorption behavior of PEI(30)-Mg_2(dobpdc) will be discussed in the later section. For TEPA(50)-Mg_2(dobpdc), a strong dependence of the CO_2 adsorption capacity on the relative humidity (RH) was observed (the CO_2 adsorption capacity decreases as humidity decreases at 25 °C) with relatively stable cycle performance (the decrease in CO_2 uptake of ~9% after the first cycle of humid DAC experiments in Fig. 2b is likely due to the evaporation of small molecular amines, as tetraethylenepentamine (TEPA) is a mixture of small aliphatic amines, as noted by the vendor). Two possible causes of this strong humidity dependence are changes in the adsorption chemistry with humidity and/or enhanced diffusion due to the freeing of amines originally constrained by amine–amine hydrogen bonds in dry conditions.[15–17]

To investigate changes in the chemical state(s) of the adsorbed CO_2, *in situ* IR experiments were conducted, as shown in Fig. 3. IR peak assignments and references are tabulated in Table 1. Throughout the different humidity conditions ranging from 0% to 70% RH at 25 °C, ammonium carbamate formation (mainly two $\delta_{as}NH^{3+}$ from ammonium ions, νCOO^-, and $NCOO^-$ skeletal vibrations from carbamate ions at 1650, 1546, 1490, and 1330 cm^{-1}, respectively) were the dominant species detected, without emergence of new peaks, suggesting the same CO_2 adsorption mechanism occurred regardless of the humidity level at 25 °C.[18–32] This suggests that the role of water in enhancing CO_2 adsorption in TEPA(50)-Mg_2(dobpdc) is mainly the improvement of the diffusion of CO_2 through the 1D pores of Mg_2(dobpdc) in the presence of water vapor and the freeing of amine sites rather than changing the chemistry of the amine and CO_2 interactions.

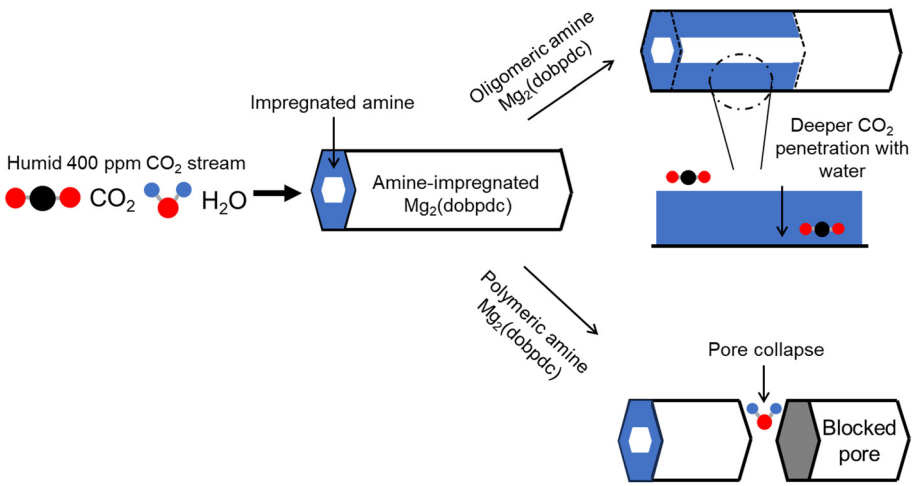

Fig. 1 Schematic illustration of the differing water effects in amine-impregnated Mg_2(dobpdc). Water increases CO_2 uptake in oligomeric amine (TEPA) impregnated Mg_2(dobpdc) by increasing CO_2 diffusion into the amine films, whereas water decreases CO_2 uptake in polymeric amine (PEI) analogue by Mg_2(dobpdc) particle/pore collapse.

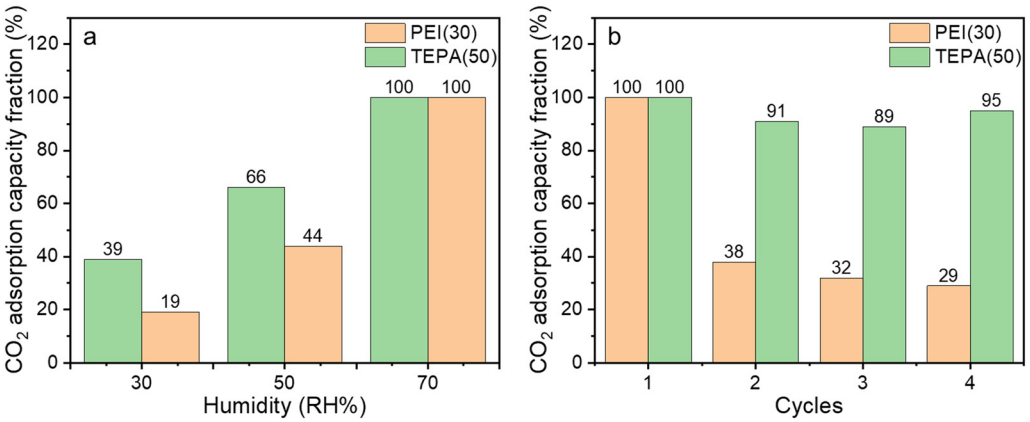

Fig. 2 Results of breakthrough experiments for BPEI(30)-Mg_2(dobpdc) and TEPA(50)-Mg_2(dobpdc) under (a) different humidities (30–70% RH) with 400 ppm CO_2/N_2 at 25 °C and (b) cycles at 70% RH. The samples were desorbed at 80 °C for 3 h under 40 sccm of N_2. The flow rate of 400 ppm CO_2 was 22 sccm and particles between 125 and 425 μm were sieved and used for the experiments (data correspond with Fig. S16†). At 70% RH and for the first cycle, CO_2 capacities of PEI(30)-Mg_2(dobpdc) and TEPA(50)-Mg_2(dobpdc) were 2.5 and 3.9 mmol g^{-1}, respectively (Table S4†).

To further investigate the role of water in the amine-impregnated Mg_2(dobpdc) materials, water isotherms (30 °C) and water uptakes (25 °C) during fixed bed experiments were measured, as shown in Fig. 4a. The water uptake increased in both the isotherm and the fixed bed adsorption experiments (25 °C) over the range of humidities studied (0 to 80%). At higher RH, the water uptake from the fixed bed experiment starts to asymptote near 15 mmol g^{-1}. In Fig. 4b, the *y*-axis in Fig. 4a is replotted as the ratio of adsorbed water to amines in TEPA(50)-Mg_2(dobpdc). At 50% RH, the adsorbed water and amine ratio becomes ~1.0, indicating equimolar levels of amines in TEPA and water. Given that the TEPA(50)-Mg_2(dobpdc) breakthrough profile at 30% RH (Fig. S16†) showed a short breakthrough time with a long mass transfer zone compared to breakthrough profiles for the same material at higher RH, we hypothesize that the hydration of TEPA significantly improves the access of CO_2 to free amine chains, and that this increase in uptake coincides with the amount of adsorbed water approaching and matching the amine loading on the adsorbent.

To separate CO_2 and water co-adsorption from the adsorption breakthrough profiles, humid 400 ppm CO_2 breakthrough profiles were measured after water presaturation, as shown in Fig. S18.† Although the breakthrough profile at 30% RH with presaturation became sharper than the co-adsorption breakthrough profile (Fig. S16b†), the pseudo equilibrium CO_2 capacity (0.74 mmol g^{-1}) decreased by 31% compared to the co-adsorption mode (1.07 mmol g^{-1}), probably due to the water molecules from the presaturation stage occupying or blocking adsorption sites for CO_2, but having overall insufficient humidity to effectively free the hydrogen-bonded amine chains. However, breakthrough profiles at higher RH (≥50%) showed pseudo equilibrium CO_2 adsorption capacities comparable to their capacities measured in co-adsorption mode (2.66 and 2.48 mmol g^{-1} at 50% RH, respectively for presaturation and co-adsorption) as well as sharp breakthrough slopes, suggesting the hydration of TEPA enabled additional CO_2–amine interactions that were not accessible at lower humidities, presumably by untangling amine–amine bonds and enhancing CO_2 access to amines deeper inside the Mg_2(dobpdc) pore.[16]

TPD results also corroborate that amines that are not accessible without hydration become accessible as humidity increases, showing a larger amount of CO_2 desorbed and concomitant delayed desorption time with increased humidity (Fig. 5). In both the water and CO_2 desorption profiles, physisorbed species desorb during the N_2 purge at 25 °C (denoted as stage I). Upon temperature ramping in stage II, the rest of the water and weekly bound CO_2 leave the system, rendering the sorbent nearly fully dried after stage II. Provided that water completely desorbs in this stage, and the amount of CO_2 desorbed is proportional to the humidity level during the adsorption stage, the CO_2 desorption peak from stage II is attributed to the water-involved CO_2 adsorbed species, such as bicarbonate‡ and hydronium carbamate (carbamic acid is excluded due to the absence of the relevant IR peaks from Fig. 3).[16,33] Surprisingly, in Fig. 5b stage III, the CO_2 desorption peak displays a delayed desorption trend as the humidity increases. Two hypotheses to explain this unexpected phenomenon are (1) an increase in the concentration of strongly bound adsorbed species and/or (2) deeper penetration of CO_2 inside the amine film with increased humidity, resulting in a longer desorption path for CO_2. The first hypothesis is not favored due to the weaker binding energy of water-involved CO_2 adsorption species such as bicarbonate and hydronium carbamate.[33] Disappearance of the later desorption

‡ While carbamic acids are readily observed in dry (primarily) and humid (occasionally) supported amine/CO_2 systems *via* IR spectroscopy, bicarbonate species are rarely observed by IR, even when the conditions are ripe for their formation. This may be associated with differing extinction coefficients for the various species. Given the large increase in CO_2 update under humid conditions observed here, we cannot fully rule out bicarbonate formation, despite no evidence for its formation by vibrational spectroscopy.

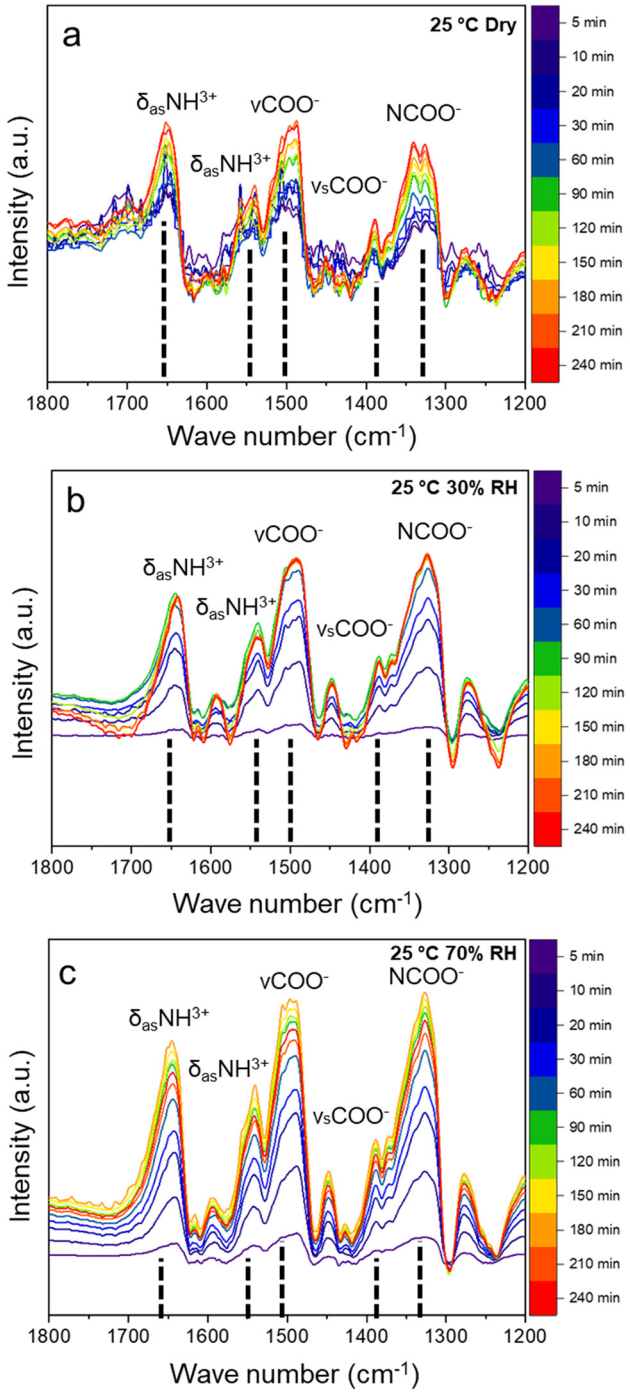

Fig. 3 *In situ* IR spectra for TEPA(50)-Mg_2(dobpdc) during 400 ppm CO_2 adsorption at 25 °C under (a) dry (b) 30, and (c) 70% RH (H_2O/CO_2 co-adsorption after H_2O presaturation) conditions.

peak at slower ramping rates (0.1 and 0.3 °C min^{-1} compared to 0.5 °C min^{-1}) during TPD experiments, as shown in Fig. S19,† corroborates that the seemingly two separate desorption peaks displayed in Fig. 5b are a result of kinetic and/or diffusion limitations rather than species with different heats of desorption. Further delayed and lengthened desorption peaks shown in Fig. S20† at a larger particle size (125–425 *vs.* 425–825 μm) at the same ramping rate (0.5 °C min^{-1}) during TPD

Table 1 *In situ* IR peak assignments during 400 ppm CO_2 adsorption at different humidities

Wave number (cm^{-1})	Assignment	Ref.
1650	$\delta_{as}NH^{3+}$	18–23
1539–46	$\delta_{as}NH^{3+}$	18, 22, 24–27
1490–1506	νCOO^-	19, 22, 28
1450	$\delta_{s}NH^{3+}$	25
1372, 1389	$\nu_{s}COO^-$	18, 22, 25, 27, 29
1330–40	$NCOO^-$ skeletal vibrations	19–21, 23, 24, 30–32, 30–32

experiments clearly indicate that the desorption kinetics of the system are limited by intraparticle mass transfer resistance, derived from the resistance in the amine film in the Mg_2(dobpdc) pores. Therefore, we propose that the last desorption peak is from carbamate species and the desorption was slowed due to the formation of carbamate species deeper inside the amine film under humid conditions. We further suggest that the desorption of water during stage II contributes to this delayed desorption by closing the water-facilitated diffusion path and rigidifying the amine film, akin to the diffusion limited adsorption under dry conditions, as schematically explained in Fig. 6. The schematic illustration summarizes our hypothesis that CO_2 cannot diffuse deeply inside of the amine film at dry or low humidity (30% RH) conditions, but the hydration of TEPA at higher humidities (≥50% RH) enables CO_2 diffusion deeper into the amine film followed by adsorption. Then, during desorption, the high CO_2 loading, including occupation of sites deep within the amine film, causes a longer desorption diffusion time due to the carbamate formation deep inside amine film along with the removal of the facilitated diffusion path for CO_2 during desorption by water.

In the last decade, studies with different types of support materials and amines suggested the observed improvement of CO_2 uptake in the presence of water can be attributed to the enhancement in CO_2 diffusion, increased amine availability, and sometimes, altered adsorption chemistry, as summarized in Sayari's review paper.[17] With additional focus on DAC, we tabulated the dry and humid CO_2 adsorption performance of different solid supported amines under DAC conditions in Table S5.† Importantly, a recent study by Hoffman *et al.* clearly reported that humidity improves the 400 ppm CO_2 uptake of PEI films by reducing their diffusion resistance as shown using their customized tandem QCM/PM-IRRAM apparatus.[34] This observation, combined with our findings, suggests that DAC adsorbents previously excluded from consideration for practical deployment due to their low CO_2 uptake under relatively dry conditions (<50% RH) may require reevaluation at higher humidity conditions. We expect that this enhancement in the CO_2 uptake kinetics in the presence of humidity will be more prominent in support materials with one dimensional pores due to their long diffusional path, as reported by Heydari-Gorji *et al.*, compared to those supports with multidimensional connections.[35]

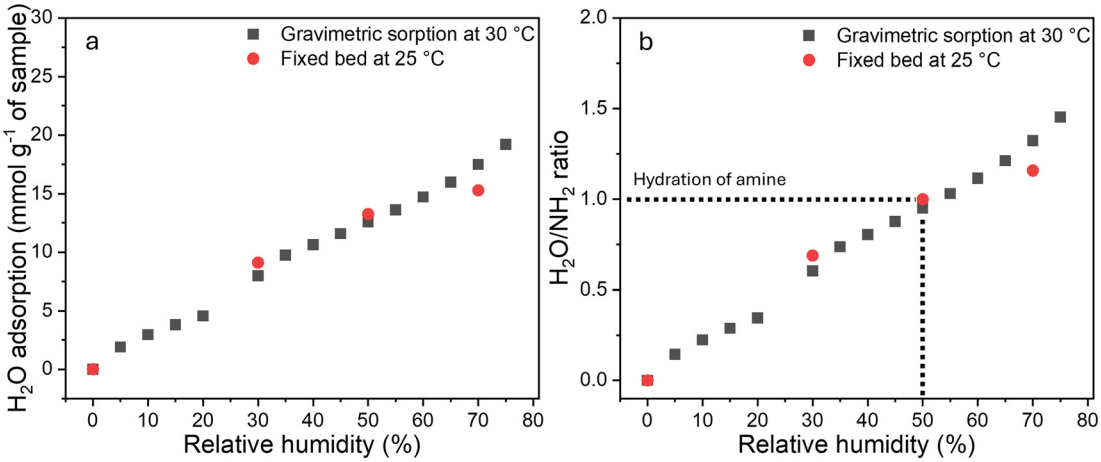

Fig. 4 TEPA(50)-Mg_2(dobpdc) (a) water uptake by gravimetric sorption (30 °C) and fixed bed experiments (25 °C); the water uptake was converted into (b) the ratio of water and amine.

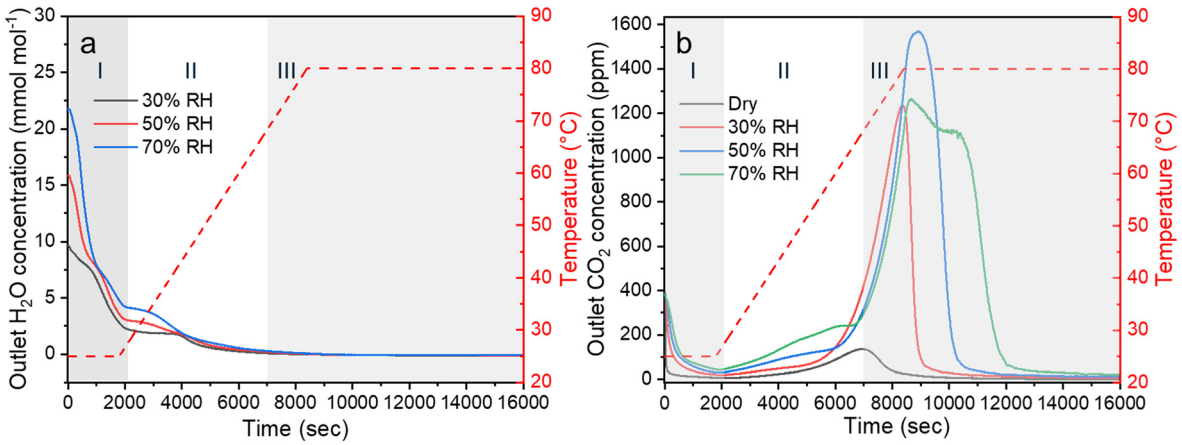

Fig. 5 Temperature programmed desorption profiles of (a) H_2O and (b) CO_2 after adsorption (400 ppm CO_2/N_2) at different humidities from dry to 70% RH for TEPA(50)-Mg_2(dobpdc). Ramping rate was 0.5 °C min^{-1} and 60 sccm of dry N_2 was used to purge desorbed gases. I: Purging stage at 25 °C under N_2; II: drying stage during temperature ramping under N_2; III: CO_2 desorption stage after water desorption.

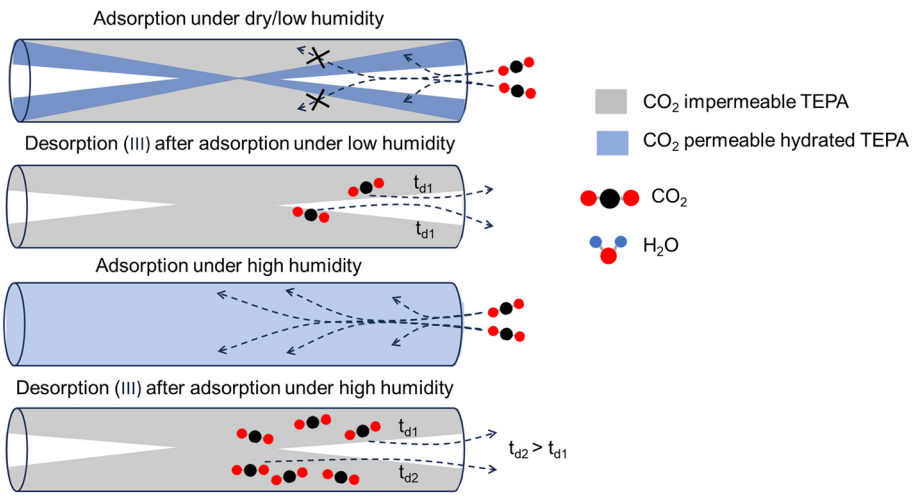

Fig. 6 Schematic illustration of CO_2 adsorption/desorption of TEPA-impregnated Mg_2(dobpdc) under different humidities during adsorption. The annotations t_{d1} and t_{d2} represent desorption time for CO_2 desorbed from surface and buried amines, respectively. CO_2 desorption time from the surface amines should be faster than that from amines buried under surface amines.

Decreased CO_2 adsorption capacity of polymeric amine-impregnated Mg_2(dobpdc) under humid DAC conditions: water-induced structural disorder

Branched PEI (BPEI)-impregnated Mg_2(dobpdc) was prepared and tested under humid DAC conditions as well. In contrast to the TEPA case discussed above (Fig. 1 and S16†), a decrease in the CO_2 capture capacity for BPEI(30)-Mg_2(dobpdc) was observed after humid cycling at 25 °C and 70% RH, as shown in Fig. 2b and S16.† Two hypotheses were put forth to explain this performance degradation. The first hypothesis was a loss of amines needed to adsorb CO_2 due to the evaporation of amines during regeneration. Recently, Mahajan *et al.* reported the degradation of the CO_2 adsorption capacity of ethylenediamine functionalized Mg_2(dobdc) (MOF-74) due to the loss of ethylenediamine over humid (65% RH humidity at 25 °C) DAC cycles.[36] However, in our case, similar combustion TGA profiles (Fig. S21a†) before and after humid cycling do not support an extensive loss of the low volatility BPEI amines. The second hypothesis was MOF framework degradation due to the extensive interaction with water during humid cycles. In Fig. S21b,† *in situ* IR spectra of the freshly activated sample subtracted from the activated BPEI(30)-Mg_2(dobpdc) after each humid 400 ppm CO_2 adsorption (30 °C, 50% RH) and desorption (80 °C and N_2 for 2 h) cycle are shown. Interestingly, the subtracted spectra displayed two distinct peaks, positive at 1682 cm^{-1} and negative at 1021 cm^{-1}. The bending mode of the water molecules [$\beta(H_2O)$] corresponding to an 18 cm^{-1} blue shift from that of water molecules adsorbed in the Mg-MOF-74 (1663 cm^{-1} at 24 °C) suggests liquid-like water formation rather than gas phase water (~1590 cm^{-1}) in the BPEI impregnated Mg_2(dobpdc) channels, even after activation.[37,38] The red shift (1682 to 1680 cm^{-1}) of this $\beta(H_2O)$ peak as the cycling evolved represents a decrease in water hydrogen bonding and redistribution of water either in the Mg_2(dobpdc) framework or amine domains.[39,40] While several possibilities (C–C, C–O, and C–N) for the negative peak at 1020 cm^{-1} exist due to the highly overlapping nature of various bands in this wave number range (the fingerprint region, 600–1400 cm^{-1}), we suggest that large BPEI polymer coils, whose radii of gyration (~1.4 nm) are larger than the pore radius of Mg_2(dobpdc) (1.05 nm), could not stabilize the open metal sites of Mg_2(dobpdc) effectively and this led to the occurrence of metal-linker hydrolysis reactions upon exposure to the humid conditions.[6,40–42] From powder X-ray diffraction (PXRD) patterns shown in Fig. S22,† a slight decrease in the peak intensity at 2θ = 4.9° was observed for both BPEI(30) and TEPA(50)-Mg_2(dobpdc), representing disorder in the translational symmetry of the hexagonal Mg_2(dobpdc) (210) plane upon exposure to ambient air.[40] A significant decrease in the BET surface area for both materials was also measured (Fig. S23†), attributed to either pore blockage by pore/particle collapse or amine redistribution.

While these observations do not give clear insight into the differing stability of BPEI(30)-Mg_2(dobpdc) and TEPA(50)-Mg_2(dobpdc), SEM images before and after humid cycles provided a clear contrast between these samples, as shown in Fig. 7. Damage on the surface of bare Mg_2(dobpdc) and BPEI(30)-Mg_2(dobpdc) after 5 humid fixed bed adsorption and desorption cycles was observed, unlike in the TEPA(50)-Mg_2(dobpdc) case, which had a clean particle surface. This pore/particle collapse can lead to pore blockage, as reported by Vitillo *et al.*, and this can be detrimental to gas adsorption in one-dimensional pore materials.[38,43,44] Indeed, Forse *et. al.* found the diffusion coefficient of CO_2 through the wall of Mg_2(dobpdc) at 625 mbar was 30 times slower than the diffusion coefficient along the pore channel.[43] Further comparison of humid breakthrough cycles with BPEI(40)-Mg_2(dobpdc), and LPEI(40)-Mg_2(dobpdc), as shown in Fig. S24,† revealed a similar degradation in adsorption capacity, manifesting as fast CO_2 breakthroughs (low adsorption capacity) after multiple cycles. Low molecular weight (MW: 800), lab-synthesized LPEI material was used for control experiments here because we hypothesized it can better access the pores of Mg_2(dobpdc) than commercial 800 MW BPEI or 2500 MW LPEI. The similar degradation behavior observed here for these samples implies that PEI may be

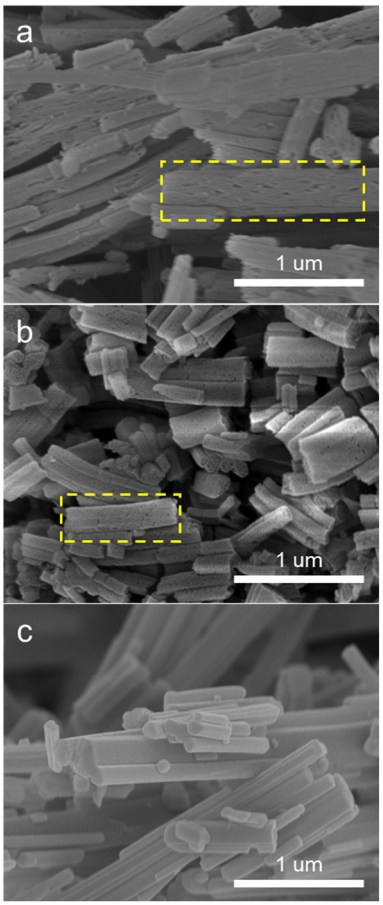

Fig. 7 SEM images of (a) bare Mg_2(dobpdc), (b) BPEI(30)-Mg_2(dobpdc), and (c) TEPA(50)-Mg_2(dobpdc) after 5 humid adsorption/desorption cycles. Adsorption and desorption conditions were 30 °C and 50% RH for 2 h with 400 ppm CO_2/N_2 and 80 °C and dry N_2 for 2 h, respectively. Perforation (yellow box) on the crystal surfaces of the (a) bare Mg_2(dobpdc) and (b) BPEI(30)-Mg_2(dobpdc) is notable.

stuck in the middle of the one-dimensional pores due to multiple interactions between amines and open metal sites within a single, (relatively) long organic chain. Based on the above observations, we conclude that the larger number of interaction points in BPEI or LPEI with Mg_2(dobpdc) open metal sites hindered the diffusion of PEI along the pore and limited the filling of amines in the pores and the coverage of open metal sites with amines. Consequently, this leads to free open metal sites and instability under humid conditions (hydrolysis of the linker and metal node),[6,40–42] leading to pore/particle collapse that causes a decrease in CO_2 adsorption capacity during cycling, as schematically illustrated in Fig. 8.

We note that TEPA-impregnated Mg_2(dobpdc) was the most resistant toward degradation from humidity among all samples, including the open metal site functionalized m-2-m-Mg_2(dobpdc), even after 40 TGA humid cycles, as judged by their SEM images (Fig. S25†). We hypothesize this is because this sample has several layers of TEPA protecting the Mg_2(dobpdc) framework. The degradation of Mg_2(dobpdc) framework may explain the compromised CO_2 adsorption capacity of m-2-m-Mg_2(dobpdc) by 30% after 5 cycles of 10% CO_2/N_2 under humid condition (73% RH) at 25 °C from the work of Adil *et al.*[45]

Practical aspects of TEPA(50)-impregnated Mg_2(dobpdc): sorption at 70% RH at 25 °C demonstrates stability over the tested cycles

The stability of TEPA(50)-Mg_2(dobpdc) over multiple humid adsorption–desorption cycles was investigated next, as shown in Fig. 9. Compared to the first cycle, the pseudo equilibrium capacities of subsequent cycles decreased modestly, by 18% (from 3.78 to 3.11 mmol g^{-1} or 0.28 to 0.23 CO_2/amine). The evaporation of low molecular weight amine species in TEPA may cause a decrease in the CO_2 adsorption capacity, as commercial TEPA is a mixture of small amines. After the first cycles, however, the TEPA(50)-Mg_2(dobpdc) showed reproducible breakthrough profiles over the period of the tests (20 cycles, roughly a month of lab scale breakthrough experiments), demonstrating its stability under practical DAC adsorption conditions, unlike the PEI analogue. For fast

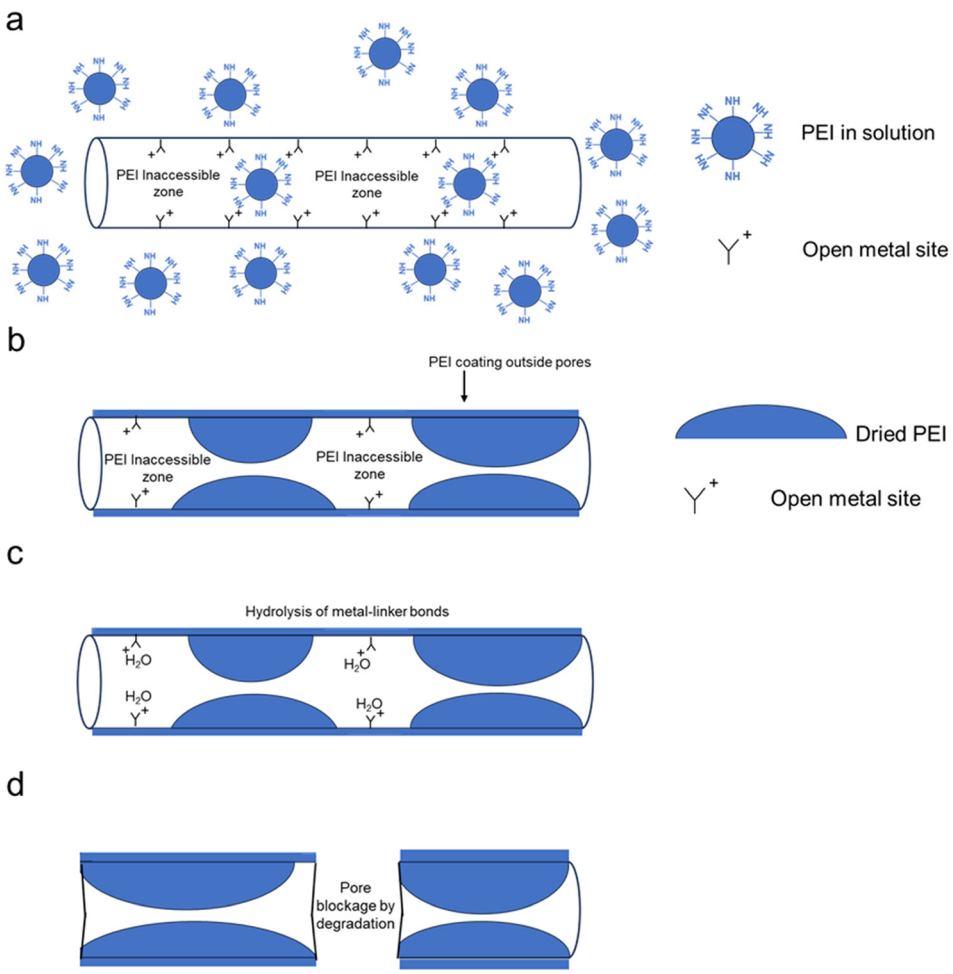

Fig. 8 Schematic illustration of the degradation of PEI-impregnated Mg_2(dobpdc) under humid adsorption conditions. (a) and (b) represent PEI distribution in the Mg_2(dobpdc) pore during the amine impregnation and after the drying step, respectively; (c) and (d) display water molecule adsorption on the Mg_2(dobpdc) open metal site and consequential pore blockage after hydrolysis, respectively.

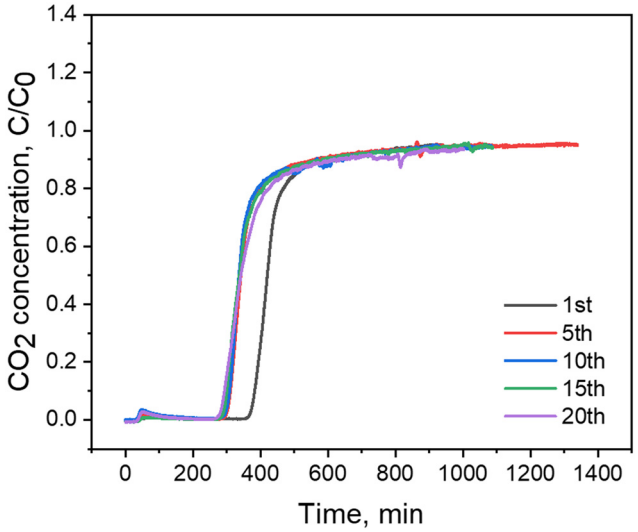

Fig. 9 Cyclic breakthrough profiles for TEPA(50)-Mg_2(dobpdc) under 70% RH with 400 ppm CO_2/N_2 at 25 °C. The sample was desorbed at 80 °C for 3 h under 40 sccm of N_2. The flow rate of 400 ppm CO_2 was 22 sccm.

cycling and scalability, steam and/or vacuum regeneration is the preferred desorption mode. In Fig. 10, vacuum desorption was chosen over steam regeneration due to the possible hydrolysis of the Mg_2(dobpdc) framework by steam.[40] Vacuum regeneration was tested using a separate vacuum oven at 0.1 bar (static) and 80 °C. Like the cyclic breakthrough experiments where a N_2 purge was used for degassing, the adsorption profiles became stable after a drop in the first cycle. On the 8th cycle, the pseudo equilibrium

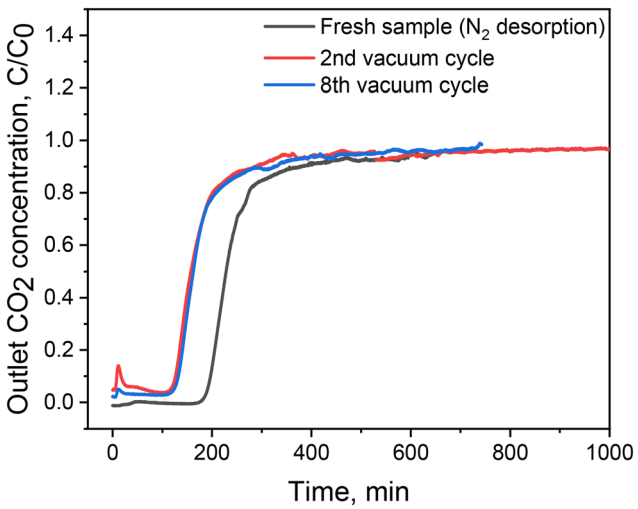

Fig. 10 Breakthrough profiles for TEPA(50)-Mg_2(dobpdc) under 70% RH and 400 pm CO_2/N_2 flow (co-adsorption) after vacuum desorption cycles. The adsorption and vacuum desorption experiment cycles consisted of exposing samples to ambient air (22 °C and 50% RH) for 20 h and desorbing adsorbates at 80 °C for 4 h under 0.1 bar static vacuum, followed by transferring the samples after certain cycles (2nd and 8th) to the fixed bed without further desorption. The flow rate was 44 sccm (400 ppm CO_2/N_2).

CO_2 capacity was recorded as 3.23 mmol g^{-1} (0.24 CO_2/amine), suggesting the potential use of the TEPA(50)-Mg_2(dobpdc) for DAC under warm and humid conditions using a temperature vacuum swing adsorption process.

3 Conclusions

The theoretical maximum amine efficiency (one CO_2 per one diamine) for chemisorption using amine-appended Mg_2(dobpdc) could not be achieved under DAC conditions, even at cold temperatures. Therefore, the amine impregnation method was used to enhance the DAC performance of sorbents based on the Mg_2(dobpdc) framework as an alternative solution. Oligomeric amine-impregnated TEPA(50)-Mg_2(dobpdc) showed a strong dependence of its adsorption and desorption performance on the humidities during adsorption. At low humidity (30% RH), the breakthrough profile of TEPA(50)-Mg_2(dobpdc) showed a long tail, indicative of diffusion-limited CO_2 adsorption behavior. However, humidities at or above equimolar TEPA hydration (water/amine = 1) conditions (≥50% RH) could facilitate CO_2 diffusion and enhance the CO_2 capture capacity of TEPA-impregnated Mg_2(dobpdc). We propose that the hydration of TEPA increases CO_2 diffusion through the amine domain, leading to more TEPA available for CO_2 as the humidity increases. Deep penetration of CO_2 into the amine domains, as evidenced by the observed delayed CO_2 desorption peak during TPD with increased humidity supports our hypothesis. On the other hand, small molecular weight (MW: 800) polymeric amine-impregnated PEI(30)-Mg_2(dobpdc) showed structural degradation (particle collapse by SEM) after exposure to the humid DAC conditions, resulting in a significant decrease in CO_2 adsorption capacity in comparison to the fresh sample (25 °C and 70% RH). Partial size exclusion of BPEI and ineffective protection of all the open metal sites in the Mg_2(dobpdc) framework were attributed as the causes of the degradation. Additional cyclic adsorption experiments with LPEI-functionalized Mg_2(dobpdc) resulted in a similar CO_2 uptake decrease, further suggesting that multiple interaction points in the PEI chain hinder PEI diffusion through the Mg_2(dobpdc) pore during synthesis, causing exposed open metal sites to exist. In contrast, 50% wt TEPA-impregnated Mg_2(dobpdc) showed outstanding CO_2 adsorption capacity and intact morphology after humid (70% RH, 25 °C) adsorption/desorption cycles. Furthermore, this TEPA-impregnated Mg_2(dobpdc) showed stable and high CO_2 capture capacity (3.2 mmol g^{-1}) over multiple cycles in a fixed bed and in vacuum desorption experiments.

Although the TEPA-impregnated Mg_2(dobpdc) showed high and reproducible CO_2 adsorption capacities under multiple humid DAC experiments, there are a few practical limitations to its potential use. First, the best-performing sample tested in this study, TEPA(50)-Mg_2(dobpdc), showed a strong dependence on the humidity of the DAC stream. The best performance was achieved at 25 °C and 70% RH among

the tested conditions. If the temperature and humidity window of effective operation cannot be extended, the locations where this adsorbent would be favorable for DAC deployment would be limited.[46,47] Furthermore, a demonstration of true long-term stability (thousands of cycles) under humidity is also needed before commercial deployment could be considered. Given that the bonds between Mg and the carboxylic acid ligand can be hydrolyzed under humid conditions, particle collapse may be unavoidable, even for the most stable TEPA(50)-Mg_2(dobpdc), under such extended cycling over long operation times (>6 months), and further testing is warranted.[48] Finally, the scalability of the Mg_2(dobpdc) is still uncertain given the instability (hydrolysis) of bare Mg_2(dobpdc) under humid conditions and limited commercial supply chains.

4 Experimental

4.1 Materials and chemicals

Solvents for material synthesis such as methanol, *N*,*N*-dimethylformamide (DMF), hexane, and anhydrous toluene were purchased from Sigma Aldrich. $Mg(NO_3)_2{\cdot}6H_2O$ from Sigma Aldrich and H_4dobpdc from Trylead Chemical Technology Co., Ltd. were used for Mg_2(dobpdc) synthesis. For amine functionalization, *N*-methylethylenediamine (m-2), *N*,*N*′-dimethylethylenediamine (m-2-m), *N*,*N*-diethylethylenediamine (ee-2), *N*,*N*-diisopropylethylenediamine (ii-2), tetraethylenepentamine (TEPA), branched poly(ethyleneimine) (BPEI) (800 Da) were acquired from Sigma Aldrich. All chemicals were used without further purification. Gases for adsorption experiments were provided by Airgas, LLC. The synthesis of linear PEI (LPEI) is described in the ESI.†

4.2 Mg_2(dobpdc) synthesis

The bare Mg_2(dobpdc) was synthesized by a gram-scale solvothermal method as previously reported.[6] The metal source $Mg(NO_3)_2{\cdot}6H_2O$ (9.89 g, 36.1 mmol) and ligand H_4-dobpdc (11.5 g, 44.9 mmol) were first dissolved in the mixture of methanol and DMF solution (55 : 45 volume fraction) *via* bath type sonication until the solution to be clear without any particulates. Subsequently, the reaction solution was transferred to a 350 mL glass pressure vessel with a Teflon screw cap and stirring bar. The reaction was conducted for 20 h at 120 °C using silicon oil bath. After naturally cooling down the reactor, the product was washed three times with 250 mL of DMF and methanol. In each step, the product was soaked by solvents for at least 3 h at 60 °C and separated by centrifugation (12 000 rpm, 15 min).

4.3 Amine-appended Mg_2(dobpdc)

Open metal site functionalization with amines was conducted as reported by Siegelman *et al.*[6] Roughly 450 mg of the methanol solvated Mg_2(dobpdc) was solvent exchanged by three times of anhydrous toluene (30 mL each) using centrifugation (12 000 rpm, 15 min). After redispersing Mg_2(dobpdc) in 120 mL of the anhydrous toluene using bath sonication for 20 min, the dispersion was transferred to 250 mL Erlenmeyer flask with Ar purge. Subsequently, amines for open metal functionalization (30 mL) such as m-2, m-2-m, ee-2, and ii-2 were added to the Mg_2(dobpdc) dispersion and sonicated for another 20 min. Without any disturbance, the reaction solution was left for 24 h at room temperature. Finally, as synthesized amine-appended Mg_2(dobpdc) was washed with 150 mL of toluene and hexane three times each.

4.4 Amine-impregnated Mg_2(dobpdc)

Roughly 450 mg of methanol-solvated Mg_2(dobpdc) was dispersed in a round bottom flask using bath type sonication for 20 min. In parallel, a targeted amount of TEPA, LPEI800, or BPEI800 was dissolved in 10 mL of methanol under the bath sonication for 20 min. Subsequently the amine solution was added to the Mg_2(dobpdc) dispersion and the mixture of the solution was stirred for 24 h at room temperature. The solid powder of amine-impregnated Mg_2(dobpdc) was obtained by evaporating methanol at 50 °C and 200 mbar using rotary evaporator.

4.5 Material characterizations

The weight fraction of amines in Mg_2(dobpdc) was determined by thermogravimetric analysis (TGA, TGA 550 TA instruments). Samples were degassed under N_2 for 2 h at 110 °C before ramping up to 800 °C. The weight fraction of amines was calculated based on the ratio of the residual weight fraction of bare Mg_2(dobpdc) and amine-functionalized Mg_2(dobpdc). X-ray diffraction (XRD) patterns for samples were measured using X'Pert PRO Alpha-1 using Cu Kα radiation. Micrographs of Mg_2(dobpdc) particles were obtained by scanning electronic microscopy (SEM) (Hitachi SU8230).

4.6 Adsorption experiments

N_2 and CO_2 adsorption isotherms were measured by a surface area and porosity (SAP) system (Autosorb IQ/Quantachrome). To degas, about 60 mg of the amine appended samples (m-2, m-2-m, ii-2, ee-2) were activated at 120 °C under vacuum (<0.1 mbar) for 12 h. For amine-impregnated (BPEI and TEPA) Mg_2(dobpdc), samples were activated at 80 °C for 4 h under the same vacuum level. The BET surface area was calculated from the N_2 physisorption data in the P/P_0 range of 0.05–0.2.[49] For CO_2 isotherms, an equilibration interval of 15 min was used throughout the whole pressure range after optimization of the equilibration time using ii-2-Mg_2(dobpdc). For the amine-impregnated samples, PEI-Mg_2(dobpdc) or TEPA-Mg_2(dobpdc), 7 min of equilibration time was allowed, resulting in at least 5 days to complete the entire measurement. Different P/P_0 tolerance was applied over the following pressure ranges: (i) $+2.5 \times 10^{-6}$ and -8.3×10^{-7} for a relative pressure range from 10^{-5} to 10^{-2}, (ii) $+3.0 \times 10^{-5}$ and -1.0×10^{-5} for a relative pressure range from 1.0 ×

10^{-2} to 2.5×10^{-2} and (iii) $+3.0 \times 10^{-3}$ and -1.0×10^{-3} for a relative pressure range from 2.5×10^{-3} to 1.

Water isotherms were obtained on a vapor sorption analyzer (VTI-SA+, TA instrument). To begin with, 30 mg of wet samples were loaded in a quartz pan and degassed at 80 or 110 °C for 4 h with dry N_2 flow. During isotherm measurements, the maximum equilibration time and tolerance were set to be 400 min and 0.0005 wt% weight change in 5 min, respectively.

Breakthrough profiles were obtained using a custom-built fixed bed system as described in our previous studies.[50,51] Briefly, adsorbent materials (60 mg, wet weight) were loaded in 1/4 inch diameter stainless tube with both ends blocked by glass wool after obtaining particles between 125 and 425 μm using sieves. The dry weight of the samples was measured in parallel by running a TGA degassing procedure on the sample from the same container right after loading the materials in the fixed bed. To start breakthrough experiments, the loaded samples were activated at 110 °C (heating tape) or 80 °C (chiller, Julabo CD-600F) until the outlet CO_2 concentration was lower than 5 ppm (typically ≤4 h) for amine appended and impregnated Mg_2(dobpdc), respectively. Before adsorption started, the fixed bed was immersed in a chiller (Julabo CD-600F) at the adsorption temperature and 10 min of thermal equilibration time was allowed. During adsorption, dry or humid 400 ppm CO_2/N_2 gas was introduced to the adsorbent bed for dry and CO_2/H_2O co-adsorption experiments. Flow rates for 400 ppm CO_2/N_2 were 22 or 44 sccm (specified in the figure captions). For presaturation experiments, wet N_2 gas (60 sccm) with specified relative humidity flowed to the bed until the inlet and outlet concentration of H_2O became equal, before passing humid 400 ppm CO_2/N_2 through the bed. Pseudo equilibrium and breakthrough capacities are defined as the captured CO_2 amount when the ratio of the outlet CO_2-concentration to inlet CO_2 concentration (C/C_0) reached 95% and 5%, respectively. The CO_2 or H_2O capacities were calculated by the integration of the area between the CO_2 or H_2O concentration profiles with and without adsorbents. The outlet CO_2 concentration was monitored by an infrared gas analyzer (LI-850/LI-COR). During 20 cyclic experiments, various humid conditions were tested in between periodic 70% RH adsorption cycles. For the cyclic experiments with vacuum desorption, several samples were stored in a vacuum oven and alternatively exposed to the ambient lab air (22 °C, 50% RH on average) for 20 h and vacuum for 4 h (80 °C, 0.1 bar static). To perform a breakthrough adsorption experiment with these vacuum-desorbed samples, one of the stored samples, after the vacuum desorption step, was transferred to the fixed bed, and wet 400 ppm CO_2/N_2 gas was introduced without additional desorption.

4.7 Spectroscopy

In situ infrared spectra of the samples under different DAC adsorption and desorption conditions were measured using a Nicolet iS10 IR spectrometer with a low-temperature diffuse reflectance infrared Fourier transform spectroscopy (DRIFTS) cell (CHC-CHA-4, Harrick Scientific Products Inc.), as shown our previous report.[52] About 50 mg of the sample was loaded in a sample holder inside the DRIFTS cell and then was activated at 80 °C under 60 sccm of N_2 flow for 4 h. Then, once the sample temperature reached the desirable adsorption temperature (−20 °C or 25 °C), the inlet gas flow was switched from N_2 to dry or wet (30% or 70% RH) 400 ppm CO_2/N_2 (40 sccm). During the adsorption and desorption steps, IR spectra were collected every 5 min with 64 scans per spectra at a resolution of 4 cm^{-1}. The humidity for the wet gas was introduced by a humidifier (WETSYS/SETARAM). For presaturation experiments, wet N_2 gas (60 sccm) was flowed first until the outlet water concentration had the same concentration as the inlet concentration using an IR CO_2/H_2O analyzer (LI-COR 850, Bioscience). After the sample was saturated with H_2O, the wet N_2 gas was switched to wet 400 ppm CO_2/N_2 gas (40 sccm). Proton T_1–T_2 correlation NMR measurements were conducted under a static N_2 environment without spinning as described in our previous publications.[53,54] Detailed experimental parameters and the data processing method for proton T_1–T_2 correlation measurements are available in the ESI.†

Data availability

The data supporting this article have been included as part of the ESI.† Raw data are available from the corresponding author upon reasonable request.

Conflicts of interest

The authors declare the following competing financial interest(s): C. W. J. has a financial interest in several DAC companies that seek to commercialize CO_2 capture from air. C. W. J. has a conflict-of-interest management plan in place at Georgia Tech.

Acknowledgements

The research was funded by Carbon Capture Inc. Some of the materials characterization such as SEM and XRD were performed in part at the Georgia Tech Institute for Electronics and Nanotechnology, a member of the National Nanotechnology Coordinated Infrastructure (NNCI), which is supported by the National Science Foundation (ECCS-2025462). RPL was supported by the Thomas C. DeLoach Jr Endowed Professorship.

References

1 X. Zhu, W. Xie, J. Wu, Y. Miao, C. Xiang, C. Chen, B. Ge, Z. Gan, F. Yang and M. Zhang, Recent advances in direct air capture by adsorption, *Chem. Soc. Rev.*, 2022, **51**, 6574–6651.
2 X. Xu, C. Song, J. M. Andrésen, B. G. Miller and A. W. Scaroni, Preparation and characterization of novel CO_2 "molecular basket" adsorbents ba sed on polymer-modified

mesoporous molecular sieve MCM-41, *Microporous Mesoporous Mater.*, 2003, **62**, 29–45.
3 J. Wang, H. Huang, M. Wang, L. Yao, W. Qiao, D. Long and L. Ling, Direct capture of low-concentration CO_2 on mesoporous carbon-supported solid amine adsorbents at ambient temperature, *Ind. Eng. Chem. Res.*, 2015, **54**, 5319–5327.
4 L. A. Darunte, A. D. Oetomo, K. S. Walton, D. S. Sholl and C. W. Jones, Direct air capture of CO_2 using amine functionalized MIL-101 (Cr), *ACS Sustainable Chem. Eng.*, 2016, **4**, 5761–5768.
5 T. M. McDonald, J. A. Mason, X. Kong, E. D. Bloch, D. Gygi, A. Dani, V. Crocella, F. Giordanino, S. O. Odoh and W. S. Drisdell, Cooperative insertion of CO_2 in diamine-appended metal-organic frameworks, *Nature*, 2015, **519**, 303–308.
6 R. L. Siegelman, T. M. McDonald, M. I. Gonzalez, J. D. Martell, P. J. Milner, J. A. Mason, A. H. Berger, A. S. Bhown and J. R. Long, Controlling cooperative CO_2 adsorption in diamine-appended Mg2 (dobpdc) metal–organic frameworks, *J. Am. Chem. Soc.*, 2017, **139**, 10526–10538.
7 E. J. Kim, R. L. Siegelman, H. Z. Jiang, A. C. Forse, J.-H. Lee, J. D. Martell, P. J. Milner, J. M. Falkowski, J. B. Neaton and J. A. Reimer, Cooperative carbon capture and steam regeneration with tetraamine-appended metal–organic frameworks, *Science*, 2020, **369**, 392–396.
8 L. A. Darunte, T. Sen, C. Bhawanani, K. S. Walton, D. S. Sholl, M. J. Realff and C. W. Jones, Moving beyond adsorption capacity in design of adsorbents for CO_2 capture from ultradilute feeds: Kinetics of CO_2 adsorption in materials with stepped isotherms, *Ind. Eng. Chem. Res.*, 2019, **58**, 366–377.
9 S. Bose, D. Sengupta, C. D. Malliakas, K. B. Idrees, H. Xie, X. Wang, M. L. Barsoum, N. M. Barker, V. P. Dravid and T. Islamoglu, Suitability of a diamine functionalized metal–organic framework for direct air capture, *Chem. Sci.*, 2023, **14**, 9380–9388.
10 J. D. Martell, P. J. Milner, R. L. Siegelman and J. R. Long, Kinetics of cooperative CO_2 adsorption in diamine-appended variants of the metal–organic framework Mg2 (dobpdc), *Chem. Sci.*, 2020, **11**, 6457–6471.
11 B. D. Marshall, A cluster based cooperative kinetic model for CO_2 adsorption on amine functionalized metal–organic frameworks, *Ind. Eng. Chem. Res.*, 2022, **61**, 18138–18145.
12 Y. Cao, F. Song, Y. Zhao and Q. Zhong, Capture of carbon dioxide from flue gas on TEPA-grafted metal-organic framework Mg_2(dobdc), *J. Environ. Sci.*, 2013, **25**, 2081–2087.
13 J. H. Choe, D. W. Kang, M. Kang, H. Kim, J. R. Park, D. W. Kim and C. S. Hong, Revealing an unusual temperature-dependent CO_2 adsorption trend and selective CO_2 uptake over water vapors in a polyamine-appended metal–organic framework, *Mater. Chem. Front.*, 2019, **3**, 2759–2767.
14 T. Gelles and F. Rezaei, Diffusion kinetics of CO_2 in amine-impregnated MIL-101, alumina, and silica adsorbents, *AIChE J.*, 2020, **66**, e16785.
15 R. B. Said, J. M. Kolle, K. Essalah, B. Tangour and A. Sayari, A unified approach to CO_2–amine reaction mechanisms, *ACS Omega*, 2020, **5**, 26125–26133.
16 A. Koutsianos, A. R. Barron and E. Andreoli, CO_2 capture partner molecules in highly loaded PEI sorbents, *J. Phys. Chem. C*, 2017, **121**, 21772–21781.
17 J. M. Kolle, M. Fayaz and A. Sayari, Understanding the effect of water on CO_2 adsorption, *Chem. Rev.*, 2021, **121**, 7280–7345.
18 Z. Bacsik, N. Ahlsten, A. Ziadi, G. Zhao, A. E. Garcia-Bennett, B. Martín-Matute and N. Hedin, Mechanisms and kinetics for sorption of CO_2 on bicontinuous mesoporous silica modified with n-propylamine, *Langmuir*, 2011, **27**, 11118–11128.
19 J. Yu and S. S. Chuang, The structure of adsorbed species on immobilized amines in CO_2 capture: An in situ IR study, *Energy Fuels*, 2016, **30**, 7579–7587.
20 X. Wang, V. Schwartz, J. C. Clark, X. Ma, S. H. Overbury, X. Xu and C. Song, Infrared study of CO_2 sorption over "molecular basket" sorbent consisting of polyethylenimine-modified mesoporous molecular sieve, *J. Phys. Chem. C*, 2009, **113**, 7260–7268.
21 Z. Bacsik, R. Atluri, A. E. Garcia-Bennett and N. Hedin, Temperature-induced uptake of CO_2 and formation of carbamates in mesocaged silica modified with n-propylamines, *Langmuir*, 2010, **26**, 10013–10024.
22 A. Danon, P. C. Stair and E. Weitz, FTIR study of CO_2 adsorption on amine-grafted SBA-15: Elucidation of adsorbed species, *J. Phys. Chem. C*, 2011, **115**, 11540–11549.
23 W. C. Wilfong, C. S. Srikanth and S. S. Chuang, In situ ATR and DRIFTS studies of the nature of adsorbed CO_2 on tetraethylenepentamine films, *ACS Appl. Mater. Interfaces*, 2014, **6**, 13617–13626.
24 S. A. Didas, M. A. Sakwa-Novak, G. S. Foo, C. Sievers and C. W. Jones, Effect of amine surface coverage on the co-adsorption of CO_2 and water: Spectral deconvolution of adsorbed species, *J. Phys. Chem. Lett.*, 2014, **5**, 4194–4200.
25 G. S. Foo, J. J. Lee, C. H. Chen, S. E. Hayes, C. Sievers and C. W. Jones, Elucidation of surface species through in situ FTIR spectroscopy of carbon dioxide adsorption on amine-grafted SBA-15, *ChemSusChem*, 2017, **10**, 266–276.
26 J.-B. Bossa, F. Borget, F. Duvernay, P. Theulé and T. Chiavassa, Formation of neutral methylcarbamic acid ($CH_3NHCOOH$) and methylammonium methylcarbamate [$CH_3NH_3^+$][$CH_3NHCO_2^-$] at low temperature, *J. Phys. Chem. A*, 2008, **112**, 5113–5120.
27 J.-B. Bossa, P. Theulé, F. Duvernay, F. Borget and T. Chiavassa, Carbamic acid and carbamate formation in NH: CO ices–UV irradiation versus thermal processes, *Astron. Astrophys.*, 2008, **492**, 719–724.
28 U. Tumuluri, M. Isenberg, C.-S. Tan and S. S. Chuang, In situ infrared study of the effect of amine density on the nature of adsorbed CO_2 on amine-functionalized solid sorbents, *Langmuir*, 2014, **30**, 7405–7413.
29 C. Knofel, C. Martin, V. Hornebecq and P. L. Llewellyn, Study of carbon dioxide adsorption on mesoporous aminopropylsilane-functionalized silica and titania combining microcalorimetry and in situ infrared spectroscopy, *J. Phys. Chem. C*, 2009, **113**, 21726–21734.

30 C. S. Srikanth and S. S. Chuang, Infrared study of strongly and weakly adsorbed CO_2 on fresh and oxidatively degraded amine sorbents, *J. Phys. Chem. C*, 2013, **117**, 9196–9205.
31 A. Babin, C. Vaneeckhaute and M. C. Iliuta, Potential and challenges of bioenergy with carbon capture and storage as a carbon-negative energy source: A review, *Biomass Bioenergy*, 2021, **146**, 105968.
32 S. Kim, J. Ida, V. V. Guliants and Y. Lin, Tailoring pore properties of MCM-48 silica for selective adsorption of CO_2, *J. Phys. Chem. B*, 2005, **109**, 6287–6293.
33 J. Yu, Y. Zhai and S. S. Chuang, Water enhancement in CO_2 capture by amines: An insight into CO_2–H_2O interactions on amine films and sorbents, *Ind. Eng. Chem. Res.*, 2018, **57**, 4052–4062.
34 J. R. Hoffman, A. E. Baumann and C. M. Stafford, The role of humidity in enhancing CO_2 capture efficiency in polyethyleneimine thin films, *Chem. Eng. J.*, 2025, **507**, 160347.
35 A. Heydari-Gorji, Y. Yang and A. Sayari, Effect of the pore length on CO_2 adsorption over amine-modified mesoporous silicas, *Energy Fuels*, 2011, **25**, 4206–4210.
36 S. Mahajan, J. Elfving and M. Lahtinen, Evaluating the viability of ethylenediamine-functionalized Mg-MOF-74 in direct air capture: The challenges of stability and slow adsorption rate, *J. Environ. Chem. Eng.*, 2024, **12**, 112193.
37 K. Tan, N. Nijem, Y. Gao, S. Zuluaga, J. Li, T. Thonhauser and Y. J. Chabal, Water interactions in metal organic frameworks, *CrystEngComm*, 2015, **17**, 247–260.
38 T. Seki, K. Y. Chiang, C. C. Yu, X. Yu, M. Okuno, J. Hunger, Y. Nagata and M. Bonn, The bending mode of water: A powerful probe for hydrogen bond structure of aqueous systems, *J. Phys. Chem. Lett.*, 2020, **11**, 8459–8469.
39 M. Praprotnik, D. Janežič and J. Mavri, Temperature dependence of water vibrational spectrum: A molecular dynamics simulation study, *J. Phys. Chem. A*, 2004, **108**, 11056–11062.
40 K. Tan, S. Zuluaga, Q. Gong, P. Canepa, H. Wang, J. Li, Y. J. Chabal and T. Thonhauser, Water reaction mechanism in metal organic frameworks with coordinatively unsaturated metal ions: MOF-74, *Chem. Mater.*, 2014, **26**, 6886–6895.
41 I. I. H. Park and E. J. Choi, Characterization of branched polyethyleneimine by laser light scattering and viscometry, *Polymer*, 1996, **37**, 313–319.
42 S. Zuluaga, E. M. Fuentes-Fernandez, K. Tan, F. Xu, J. Li, Y. J. Chabal and T. Thonhauser, Understanding and controlling water stability of MOF-74, *J. Mater. Chem. A*, 2016, **4**, 5176–5183.
43 A. C. Forse, M. I. Gonzalez, R. L. Siegelman, V. J. Witherspoon, S. Jawahery, R. Mercado, P. J. Milner, J. D. Martell, B. Smit and B. Blümich, Unexpected diffusion anisotropy of carbon dioxide in the metal–organic framework Zn2 (dobpdc), *J. Am. Chem. Soc.*, 2018, **140**, 1663–1673.
44 J. G. Vitillo and S. Bordiga, Increasing the stability of Mg2 (dobpdc) metal–organic framework in air through solvent removal, *Mater. Chem. Front.*, 2017, **1**, 444–448.
45 K. Adil, P. M. Bhatt, Y. Belmabkhout, S. M. T. Abtab, H. Jiang, A. H. Assen, A. Mallick, A. Cadiau, J. Aqil and M. Eddaoudi, Valuing metal–organic frameworks for postcombustion carbon capture: A benchmark study for evaluating physical adsorbents, *Adv. Mater.*, 2017, **29**, 1702953.
46 X. Cai, M. A. Coletti, D. S. Sholl and M. R. Allen-Dumas, Assessing Impacts of Atmospheric Conditions on Efficiency and Siting of Large-Scale Direct Air Capture Facilities, *JACS Au*, 2024, **4**, 1883–1891.
47 H. Jung, K. Kim, J. Jeong, A. Jamal, D.-Y. Koh and J. H. Lee, Exploring the impact of hourly variability of air condition on the efficiency of direct air capture, *Chem. Eng. J.*, 2025, 160840, in press.
48 F. Bisotti, K. A. Hoff, A. Mathisen and J. Hovland, Direct Air capture (DAC) deployment: A review of the industrial deployment, *Chem. Eng. Sci.*, 2024, **283**, 119416.
49 K. S. Walton and R. Q. Snurr, Applicability of the BET method for determining surface areas of microporous metal – organic frameworks, *J. Am. Chem. Soc.*, 2007, **129**, 8552–8556.
50 G. Rim, F. Kong, M. Song, C. Rosu, P. Priyadarshini, R. P. Lively and C. W. Jones, Sub-ambient temperature direct air capture of CO_2 using amine-impregnated MIL-101 (Cr) enables ambient temperature CO_2 recovery, *JACS Au*, 2022, **2**, 380–393.
51 M. Song, G. Rim, F. Kong, P. Priyadarshini, C. Rosu, R. P. Lively and C. W. Jones, Cold-temperature capture of carbon dioxide with water coproduction from air using commercial zeolites, *Ind. Eng. Chem. Res.*, 2022, **61**, 13624–13634.
52 G. Rim, P. Priyadarshini, M. Song, Y. Wang, A. Bai, M. J. Realff, R. P. Lively and C. W. Jones, Support pore structure and composition strongly influence the direct air capture of CO_2 on supported amines, *J. Am. Chem. Soc.*, 2023, **145**, 7190–7204.
53 H. J. Moon, J.-M. Carrillo, J. Leisen, B. G. Sumpter, N. C. Osti, M. Tyagi and C. W. Jones, Understanding the impacts of support–polymer interactions on the dynamics of poly(ethyleneimine) confined in mesoporous SBA-15, *J. Am. Chem. Soc.*, 2022, **144**, 11664–11675.
54 H. J. Moon, R.-S. Sekiya and C. W. Jones, Probing the morphology and mobility of amines in porous silica CO_2 sorbents by ^1H T_1–T_2 relaxation correlation NMR, *J. Phys. Chem. C*, 2023, **127**, 11652–11665.